Extensive Sub-RPE Complement Deposition in a Nonhuman Primate Model of Early-Stage Diabetic Retinopathy

Shuxin Fan, Ziqi Yang, Yan Liu, Jiawei Zhong, Shuyao Zhang, Yuhua Xiao, Xu Liu, Wei Yi, Chang He, Youjin Hu, and Xialin Liu

State Key Laboratory of Ophthalmology, Zhongshan Ophthalmic Center, Sun Yat-sen University, Guangzhou, China

Correspondence: Youjin Hu, State Key Laboratory of Ophthalmology, Zhongshan Ophthalmic Center, Sun Yat-sen University, Guangzhou, 510060, China; huyoujin@gzzoc.com.
Chang He, State Key Laboratory of Ophthalmology, Zhongshan Ophthalmic Center, Sun Yat-sen University, Guangzhou, 510060, China; hech33@mail.sysu.edu.cn.

Received: September 14, 2020
Accepted: March 1, 2021
Published: March 22, 2021

Citation: Fan S, Yang Z, Liu Y, et al. Extensive sub-RPE complement deposition in a nonhuman primate model of early-stage diabetic retinopathy. *Invest Ophthalmol Vis Sci.* 2021;62(3):30. https://doi.org/10.1167/iovs.62.3.30

Purpose. This study aims to reveal retinal abnormities in a spontaneous diabetic nonhuman primate model and explore the mechanism of featured injuries.

Methods. Twenty-eight cynomolgus monkeys were identified to suffer from spontaneous type 2 diabetes from a colony of more than eight-hundred aged monkeys, and twenty-six age-matched ones were chosen as controls. Their blood biochemistry profiles were determined and retinal changes were examined by multimodal imaging, hematoxylin and eosin staining, and immunofluorescence. Retinal pigment epithelium (RPE) cells were further investigated by RNA sequencing and computational analyses.

Results. These diabetic monkeys were characterized by early retinal vascular and neural damage and dyslipidemia. The typical acellular capillaries and pericyte ghost were found in the diabetic retina, which also exhibited reduced retinal nerve fiber layer thickness compared to controls (all $P < 0.05$). Of note, distinct sub-RPE drusenoid lesions were extensively observed in these diabetic monkeys (46.43% vs. 7.69%), and complements including C3 and C5b-9 were deposited in these lesions. RNA-seq analysis revealed complement activation, AGE/RAGE activation and inflammatory response in diabetic RPE cells. Consistently, the plasma C3 and C4 were particularly increased in the diabetic monkeys with drusenoid lesions ($P = 0.028$ and 0.029).

Conclusions. The spontaneous type 2 diabetic monkeys featured with early-stage retinopathy including not only typical vascular and neural damage but also a distinct sub-RPE deposition. The complement activation of RPE cells in response to hyperglycemia might contribute to the deposition, revealing an unrecognized role of RPE cells in the early-stage pathological process of diabetic retinopathy.

Keywords: nonhuman primate (NHP), diabetic retinopathy (DR), retinal pigment epithelium (RPE), complement deposition, multimodal imaging

Diabetic retinopathy (DR) is the leading cause of irreversible blindness in working-age adults worldwide.[1] The extensive application of diabetic animal models facilitates us to get a comprehensive understanding of the pathogenesis of DR. Most animal models of DR are induced by chemicals or genetically modified.[2,3] Particularly, nonhuman primates (NHPs) could spontaneously develop type 2 diabetes, and their characteristics might exactly mimic the pathogenesis of clinical diabetes in humans.[3–6] In addition, NHP is considered to be a powerful model of ocular diseases owing to its high structural resemblance to human.[7,8] With this appropriate model, we have observed some of the vascular complications that occur in DR patients.[9–11]

Recognition of early-stage DR characteristics and understanding of the mechanism underlying the initiation of DR are essential for the prevention and control of this disease.[12,13] Previous reports on NHP model presented some signs of nonproliferative DR in humans such as microaneurysms and hard exudate.[10,11] This microvascular damage is characterized by thickening of the capillary wall, loss of pericytes, leukocyte adhesion, and progressive endothelial cell loss.[9–11,14] However, whether other retinal cells are injured in early-stage DR remain unclear and need to be clarified.

Here we first screened more than 800 cynomolgus monkeys over 15 years old by random glucose testing. After further examined by fasting glucose and HbA1c testing, 28 monkeys were diagnosed as having spontaneous type 2 diabetes. Twenty-six age-matched monkeys with normal levels of fasting glucose and HbA1c were selected as nondiabetic controls. In this study, we detected the fundus changes using multimodal imaging in these NHP models and found the spontaneous diabetic monkeys featured as typical vascular and neural damage and a remarkable drusenoid sub-RPE deposition. As we have known, drusen, the focal deposits of extracellular debris located between the RPE and Bruch's membrane, occurs naturally with age and is considered as a hallmark of age-related macular degeneration (AMD).[15,16] During the formation and development of drusen, the RPE cells recognized as injured cells would extrude unnecessary

or injured proteins and lipids in response to certain insults.[17] Here we would clarify the early damage of RPE cells at the setting of diabetes in NHP models.

Materials and Methods

Animal Handling

All animal procedures were under an experimental protocol approved by Sun Yat-Sen University's Standing Committee on Animals, as well as the tenets of the Association for Research in Vision and Ophthalmology Statement for the Use of Animals in Ophthalmic and Vision Research. The random glucose level of cynomolgus monkeys over 15 years old was preliminarily screened in individuals within two animal facilities in southern China. The spontaneous type 2 diabetes was diagnosed with positive fasting glucose and HbA1c test results. Nondiabetic age-matched controls were selected randomly from this colony. Animals with severe ocular surface disease or cataracts were excluded from this study. Age, diabetic history, and other abnormalities were carefully evaluated using the historic and medical records of each subject.

Multimodal Imaging

All of the multimodal imaging examinations were performed as previously described.[7] Briefly, the animals were sedated with 10 mg/kg 1 ketamine hydrochloride and 20 mg/kg 1 thioethamyl intramuscularly in the morning after their usual 12-hour light/12-hour dark cycle, followed by pupillary dilation with tropicamide. The head and chin rests of the imaging device (Heidelberg Engineering, Heidelberg, Germany) were removed and replaced with a custom metal bar to allow the animals' heads to rest comfortably. The ophthalmic examinations including slit-lamp biomicroscopy, color fundus photography (CFP), simultaneous fluorescein fundus angiography (FFA) and spectral domain optical coherence tomography (OCT) were performed according to the standard manufacture's protocol. Particularly, high-density (1536 A-scans/B-scan) modalities were used in spectral domain optical coherence tomography. Up to 100 scans (range, 50–100) were averaged for each B-scan, using the Heidelberg eye tracking automatic real-time software. Near-infrared fundus autofluorescence 30° images were acquired with an excitation wavelength of 787 nm. Total retinal thickness was measured at three point, the fovea pit, 2.5 mm nasal to the fovea pit, and 2.5 mm temporal to the fovea pit, and the retinal nerve fiber layer thickness was measured at the latter two positions.

Retinal Trypsin Digest and Assessment of Pericyte Loss

The retinal trypsin digest method was performed as previously described.[18] Briefly, whole retinas were dissected and fixed in 4% paraformaldehyde overnight. Then immersed in 3% trypsin (BD Bioscience, Franklin Lakes, NJ, USA) at 37°C for three hours. The isolated retinal vascular network was carefully mounted onto slides and stained with hematoxylin and eosin. Pericytes and endothelial cells were detected under the photomicroscope (Nikon, Melville, NY, USA) and counted in random fields throughout the retina. Nuclei of pericytes, which usually lie in the outer layer of the capillary wall, were identified to be more darkly-stained and smaller than endothelial cell nuclei, which were parallel to the long axis of the blood vessels. The ratio of pericytes to endothelial cells was then calculated.

Tissue Preparation and Immunofluorescence

Tissues were fixed in 4% paraformaldehyde overnight at 4°C. Cryostat sections (7 µm) were cut and mounted on coated microscopic slides. Slides were washed for 15 minutes in 0.2% potassium permanganate to eliminate autofluorescence from RPE cells and neutralized with 1% oxalic acid until the brown color was removed (30–35 seconds). Slides were put in blocking buffer (1% BSA and 0.5% Triton X-100 in PBS) for two hours at room temperature. The primary antibodies were diluted in blocking buffer and included anti-CRYAB (1:200, TA500583; Thermo Fisher Scientific, Waltham, MA, USA), anti-APOE (1:200, 16H22L18; Thermo Fisher Scientific), anti-RPE65 (1:100, ab13826; Abcam, Cambridge, MA, USA), anti-C3 (1:100, ab11871; Abcam), anti-C5b-9 (1:100, ab55811 Abcam), anti-Iba1 (1:100, 019-19741; Wako Chemicals USA, Richmond, VA, USA), anti-GFAP (1:100, ab5541; Merck Millipore, Burlington, MA, USA), and anti-RBPMS (1:100, GTX118619; GeneTex, Inc., Irvine, CA, USA). For secondary detection, Alexa Fluor–coupled secondary antibodies (1:500) were used. Cell nuclei were visualized with DAPI (0.2 µg/ml, D9542 Sigma). Negative controls for immunostaining were performed in parallel by omission of primary antibodies. Fluorescent images were taken using a confocal microscope (Olympus, Center Valley, PA, USA).

RPE Cell Isolation, RNA Extraction, Library Construction and Sequencing

RPE cells were isolated from three diabetic and three control subjects by adopting a well-established protocol. In brief, the anterior segment of monkey eyeball was cut off and removed. Then the lens, vitreous, and the sensory retina were carefully removed and the RPE cells were scraped gently from the remaining eye cup without damaging the choroid layer as far as possible. The isolated RPE cells were immediately put into the Trizol (Thermo Fisher Scientific) for RNA extraction. Total RNA was purified, and the sample quality was confirmed by the Agilent 2100 Bioanalyzer (Agilent Technology, Tokyo, Japan). Libraries were constructed using the TruSeq RNA-Seq kit (Illumina, San Diego, CA, USA) following the manufacturer's instructions. After evaluating the quality by Agilent 2100 Bioanalyzer, libraries were pooled and sequenced on Illumina Hiseq X10.

RNA-Sequencing Data Processing

The quality of all datasets was checked by FastQC (v 0.11.8), and low-quality reads were removed. Retained reads were then aligned to Macaca fascicularis genome (Macaca_fascicularis_5.0) using STAR (v 2.7.3a) in the pair-end mode with default parameters. Reads number mapped to each gene was counted using HTSeq (v 0.11.2). The output matrix from HTSeq was input into the DESeq2 (v 1.26.0) for identification of differentially expressed genes between diabetes group and control group. We determined differentially expressed genes with the criteria of absolute fold change > 2 and false discovery rate (FDR) adjusted P value < 0.05. In addition, log-fold change of all genes between two groups were used to conduct

Table 1. Characteristics of General and Blood Biochemistry Profile

	Nondiabetic ($n = 26$)	Diabetic ($n = 28$)	P
Age (years)	17.73 ± 0.73	18.11 ± 0.53	0.68
Gender (male/female)	14/12	18/10	0.58
Weight (kg)	10.80 ± 0.50	7.73 ± 0.45	<0.01
Glu (mmol/L)	4.46 ± 0.14	19.40 ± 1.22	<0.01
HbA1c (%)	3.07 ± 0.08	7.55 ± 0.22	<0.01
Ins (pmol/L)	193.04 ± 21.30	218.16 ± 73.10	0.75
CP (nmol/L)	1.43 ± 0.08	1.23 ± 0.25	0.47
LDL (mmol/L)	1.22 ± 0.11	2.18 ± 0.25	<0.01
HDL (mmol/L)	1.42 ± 0.08	1.26 ± 0.08	0.16
TG (mmol/L)	0.67 ± 0.06	5.94 ± 0.96	<0.01
TC (mmol/L)	2.99 ± 0.16	4.47 ± 0.42	<0.01
TP (g/L)	74.50 ± 0.70	77.91 ± 0.92	<0.01

CP, C-peptide; TC, total cholesterol; TG, triglyceride; TP, total protein.
* Data are mean ± SEM, with the exception of gender.
† $P < 0.05$ was considered the level of significance.

Gene Set Enrichment Analysis (GSEA), of Kyoto Encyclopedia of Genes and Genomes (KEGG) terms using clusterProfiler (v 3.14.0). All plots were generated by ggplot2 (v 3.2.1), RcolorBrewer (v 1.1-2) and clusterProfiler. Our sequencing data are available at Gene Expression Omnibus under the accession number GSE160617.

Statistical Analysis

All quantitative data are presented as means ± SEM and analyzed by a two-tailed unpaired Student's *t*-test (two groups) or one-way ANOVA (>2 groups) with a Turkey's post hoc comparisons test. $P \leq 0.05$ was considered as statistically significant.

Results

Hyperglycemia and Dyslipidemia in Cynomolgus Monkeys With Spontaneous Type 2 Diabetes

A total of 28 diabetic cynomolgus monkeys (mean age 18.11 ± 0.53 y) with a recorded diabetes duration of three to five years and 26 age-matched nondiabetic monkeys (mean age 17.73 ± 0.73 y) were studied. The characteristics of general and blood biochemistry profile of both groups were listed in Table 1. As expected, the mean fasting glucose (Glu) was 19.40 ± 1.22 mmol/L in diabetes group versus 4.46 ± 0.14 mmol/L in control group ($P < 0.01$), and the mean glycated hemoglobin (HbA1c) was 7.55% ± 0.22% in the diabetic group versus 3.07% ± 0.08 in the control group ($P < 0.01$). These diabetic cynomolgus monkeys suffered from loss of body weight and dyslipidemia with increased LDL, total cholesterol, triglyceride, and total protein, and reduced HDL (Table 1). However, the level of fasting insulin (Ins) and fasting C-peptide showed no difference between two groups ($P = 0.75$ and 0.47, respectively) (Table 1).

Retinal Vascular and Neural Degeneration in Diabetic Cynomolgus Monkeys

To comprehensively identify the diabetic damages to retina, multimodal imaging including CFP, FFA and OCT were applied on all 28 diabetic cynomolgus monkeys and 26 controls. Figures 1A to 1E showed the model examined in this study. None of these diabetic cynomolgus monkeys showed any advanced DR signs in patients such as angiogenesis or macular edema. Given the classical early-stage signs, the microaneurysms, microhemorrhages, and vascular leakage were not detected either in these diabetic monkeys (Figs. 1A–1D). However, when assessed histopathologically, the mean number of pericytes per 1000 endothelial cells in diabetic retina was significantly decreased than that in non-diabetic retinas (755.64 [range, 733.32–795.59] versus 923.74 [range, 866.71–934.87], $P = 0.018$; Fig. 2A). The microangiopathy with remarkable acellular capillaries and pericyte ghost was observed in all three trypsin-digested retinae from diabetic monkeys but not from any nondiabetic controls (Fig. 2B). These changes indicated that the diabetic cynomolgus monkeys suffered from early vascular injuries at the histopathological level that were not visible in clinical imaging.

In OCT, no remarkable retinal structural distortion was detected in both groups. At all three points, the total retinal thickness showed no difference between two groups ($P = 0.37$, 0.83 and 0.28; Table 2, Figs. 1E and 1F). However, the thickness of the retinal nerve fiber layer decreased significantly in diabetic monkeys ($P = 0.008$ and 0.04; Table 2, Figs. 1E and 1G). Histologically, the RNA-binding protein with multiple splicing (RBPMS)-positive retinal ganglion cell (RGC) cells were also reduced in diabetic retina compared with nondiabetic controls (Fig. 2E). Consistently, both Müller cells and microglia were activated in response to diabetes insult with strong staining of glial fibrillary acidic protein (GFAP) and Iba1 in the diabetic retinae (Figs. 2C, 2D). Taken together, evidence obtained from multimodal imaging and histological study identified early retinal vascular and neural damages in the diabetic cynomolgus monkeys.

Distinct Sub-RPE Drusenoid Lesions in Diabetic Cynomolgus Monkeys

Apart from those typical early diabetic injuries to the vascular and neural retina, interestingly, spheroid and white dot lesions scattered along the retinal vascular arcade were observed in about half of the diabetic subjects (13 out of 28), whereas only two of 26 controls presented with similar lesions (46.43% vs. 7.69%; Figs. 3A–3G). Most the dot lesions were around the vessels but not extended to the macular area, and they appear to be not confluent. In OCT, the white dot lesion showed a distinct small hard drusenoid

Investigative Ophthalmology & Visual Science

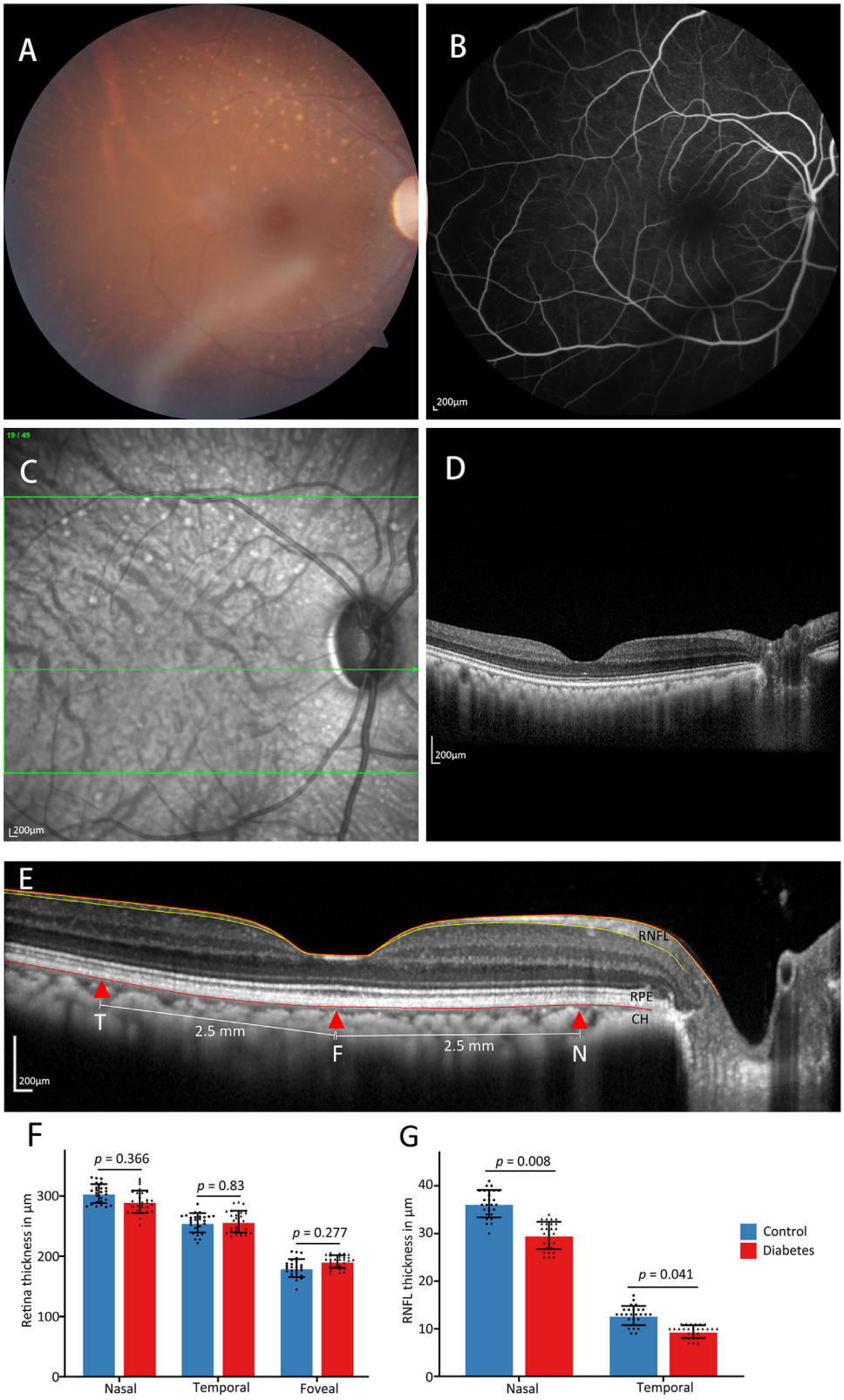

Figure 1. The retinal changes of diabetic monkey determined by multimodal imaging. (**A–D**) Multimodal imaging including color fundus photography, FFA, near-infrared, and optical coherence tomography were applied, and no obvious microaneurysms, microhemorrhages, and vascular leakage were observed in these monkeys (n = 28 diabetic monkeys, 26 controls). (**E**) Total thickness of retina was measured at three points, which is the fovea pit, 2.5 mm nasal to the fovea pit, and 2.5 mm temporal to the fovea pit (F, N and T, *red arrowheads*). In addition, the RNFL thickness was also measured at N and T locations (*red arrowheads*). (**F, G**) The total retinal thickness at all three points showed no difference between diabetic monkeys and controls ($P = 0.366$, 0.830 and 0.277), whereas the thickness of RNFL decreased significantly in diabetic monkeys ($P = 0.008$ and 0.041). n = 28 diabetic monkeys, 26 controls.

Investigative Ophthalmology & Visual Science

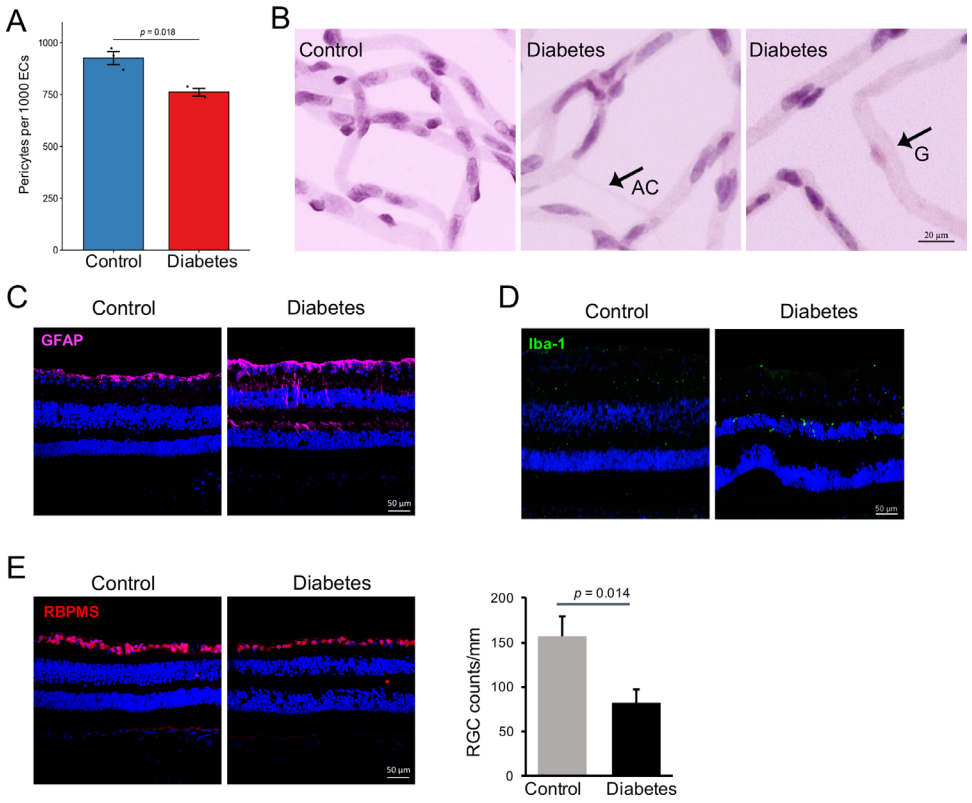

Figure 2. The vascular and neural retina were impaired histologically in the diabetic monkeys. (**A**) Mean number of pericytes per 1000 endothelial cells in diabetic retina was significantly decreased than that in nondiabetic retinas. n = 3 diabetic monkeys, 3 controls, $P = 0.018$. (**B**) Representative images of trypsin digested retinal capillary network after hematoxylin and eosin staining in both control and diabetic retina. Acellular capillaries (AC, *arrow*) and pericyte ghost (G, *arrow*) could be observed in diabetic retinae but not in controls. *Scale bar:* 20 μm. (**C**) The activation of Müller cell was detected by immunostaining of GFAP. The diabetic retina presented high expression and wide distribution of GFAP. (**D**) The microglia were also activated in response to diabetic insult with increased expression of Iba-1 in diabetic monkey. (**E**) The RBPMS-positive RGC cells were significantly decreased in the diabetic retina compared with controls, $P = 0.014$.

Table 2. Measurement and Comparison of Retinal Thickness by Optical Coherence Tomography

	Non-Diabetic ($n = 26$)	Diabetic ($n = 28$)	*P*
Total Retina Thickness (μm, 95% CI)			
Nasal	304.33 (287.36–321.30)	290.60 (256.03–325.17)	0.37
Temporal	255.83 (238.29–273.37)	257.80 (242.06–273.54)	0.83
Foveal	180.50 (161.88–199.12)	191.2 (175.31–207.09)	0.28
RNFL thickness (μm, 95% CI)			
Nasal	36.17 (33.74–38.60)	29.20 (24.78–33.62)	<0.01
Temporal	12.67 (9.65–15.68)	9.40 (7.73–11.07)	0.04

RNFL, retinal nerve fiber layer.
* $P < 0.05$ was considered the level of significance.

appearance, which was featured with RPE layer deformation and thickening (Figs. 3E and 3F). Thus these diabetic cynomolgus monkeys were featured as the presence of drusenoid changes in the retina.

RNA-Seq Revealed Complement Activation in Diabetic RPE Cells

As the drusen, focal deposits of extracellular debris, are usually associated with RPE abnormalities, we isolated RPE cells from three diabetic cynomolgus monkeys and three controls and then performed RNA-seq. Authentication of RPE cells was showed in the Supplementary Figure S1. In total, 2744 differentially expressed genes were found between the diabetic group and control. Among these differentially expressed genes, 1694 (62%) genes were upregulated in the diabetic group, and 1050 (38%) were downregulated (Fig. 4A). The top 50 upregulated and downregulated genes were listed in the Supplementary Table S1. As expected, the pathway genes involved in AGE-RAGE signaling were upregulated in diabetic RPE cells, including BCL2, BAX, ICAM1, MAPK3, and COL1A1 (Fig. 4B). Of note, we found diabetic RPE cells presented with high expression of genes involved in complement activation such as

Investigative Ophthalmology & Visual Science

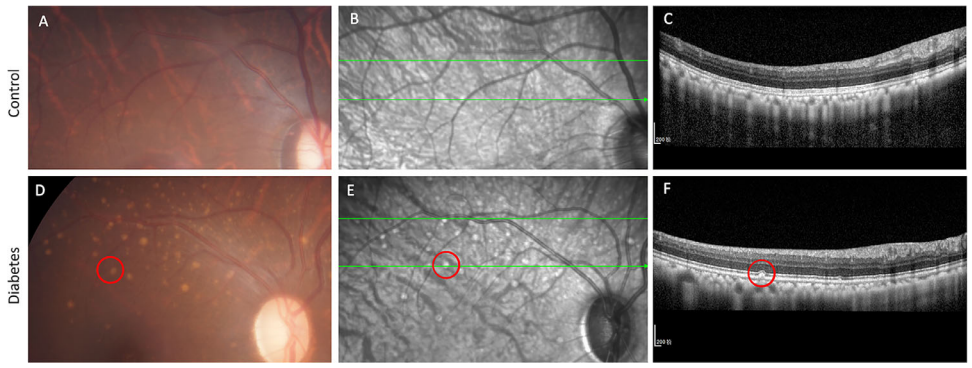

Figure 3. Diabetic monkey developed a characterized drusenoid-like deposition. (**A–C**) Color fundus photography and OCT of a nondiabetic monkey showed no abnormal appearance around the retinal vessels. (**D–G**) In over 46% of diabetic monkeys, remarkable white dot lesions could be found around the retinal vessels, whereas only 7.69% of nondiabetic monkeys present similar dot lesions. The white dot lesion in CFP (**D,** *red circle*) showed a typical drusenoid appearance beneath the retinal pigment epithelium layer in OCT (**E** and **F**, *red circle*).

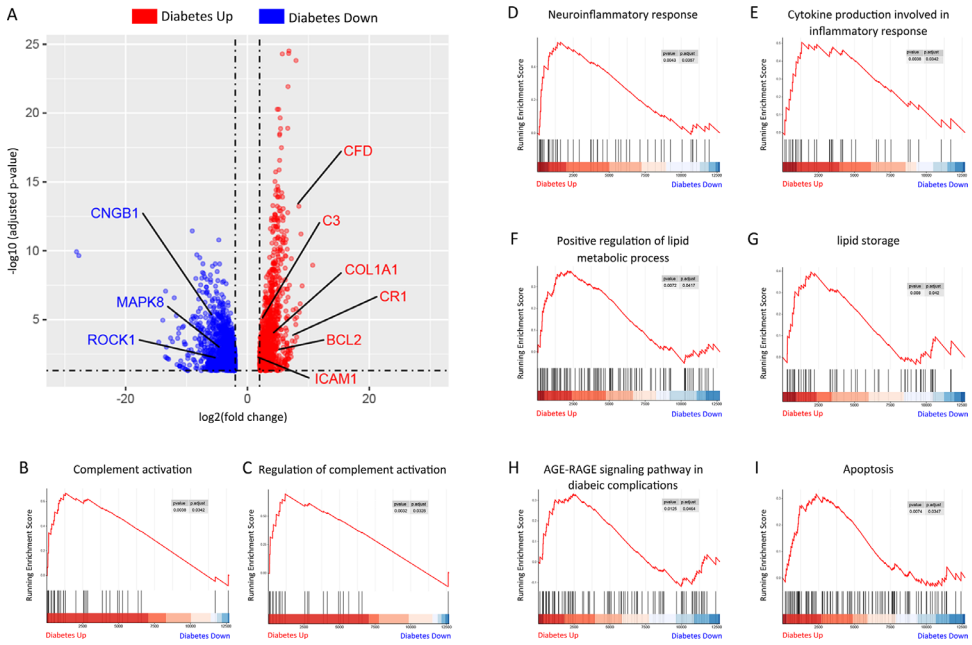

Figure 4. The transcriptional changes of RPE cells by RNA-sequencing analysis. Differential gene expression analysis for diabetic RPE versus nondiabetic control. Volcano plot of dysregulated genes at limma $P < 0.05$ (**A**). Significantly enriched gene sets (adjusted P value < 0.05), including complement activation (**B**), regulation of complement activation (**C**), neuroinflammatory response (**D**), cytokine production involved in inflammatory response (**E**), positive regulation of lipid metabolic process (**F**), lipid storage (**G**), AGE-RAGE signaling pathway in diabetic complications (**H**), and apoptosis (**I**) found by GSEA.

C3, C4BPA, C8G, CR1 and CFD, indicating both classic and alternative pathway may be activated in RPE in response to hyperglycemia insults (Fig. 4C). Furthermore, because C3a/C3aR activation could induce suppression of cAMP signaling pathway, a potent negative modulator of inflammation, we analyzed the top downregulated genes in diabetic RPE cells and found low expression of several genes in cAMP signaling like CREB3L3, HCN4, ROCK1, MAPK8 and CNGB1, indicating uncontrolled complement activation occurred in diabetic RPE cells. Besides, GSEA also revealed 85 significantly enriched gene sets including cytokine production, lipid storage, neuroinflammatory responses, and more (Figs. 4D–4I). Taken together, these findings suggested that at the setting of diabetes, RPE cells are active and possibly incline to induce inflammation via complement activation.

Sub-RPE Complement Deposition in Diabetic Retina

To further clarify the structure and composition of these drusenoid lesions, microscopic examination, hematoxylin and eosin staining and immunofluorescence were performed. The drusenoid lesions could be observed as white dots in the range of around 150 microns down to several microns in size under light microscope

Investigative Ophthalmology & Visual Science

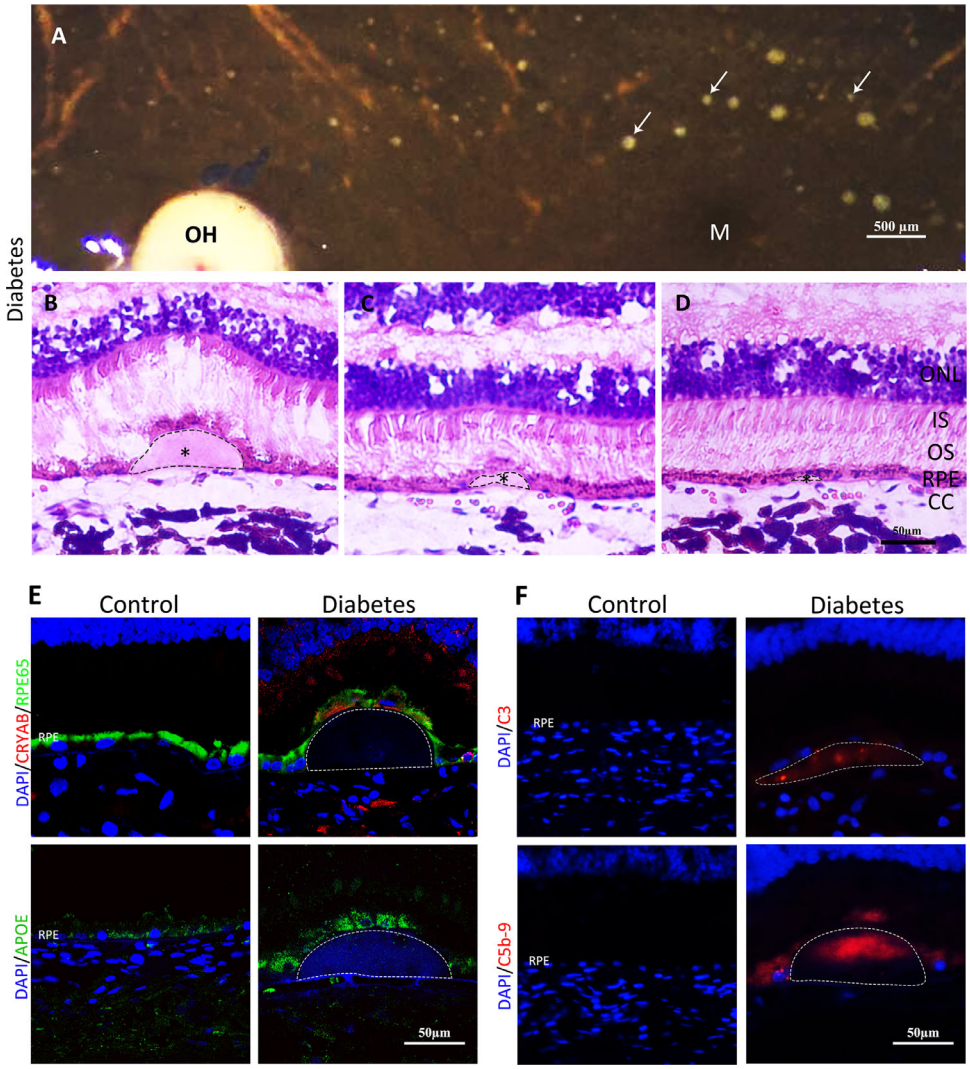

Figure 5. The histological changes of drusenoid-like deposition in diabetic monkey. (**A**) Fundus of a diabetic monkey after removing the retina, extensive white dot lesions in various sizes (*arrows*) could be observed. OH, optic head; M, macula; *Scale bar:* 500 μm. (**B–D**) Hematoxylin and eosin staining showed that the white dot lesions were pink dome-shaped and laminal sub-RPE deposits (**B**, **C**, and **D**, *dotted line*) around 150 μm down to several micrometers in size. *Scale bar:* 50 μm. (**E**) Histologic sections of retinas immunolabeled showed alpha-crystallin B chain (CRYAB) protein were expressed underneath RPE65-positive cells and above the deposits (*dotted line*) in diabetic retina. Although ApoE (*green*) could be observed in both control and diabetic retina, its expression and accumulation across the RPE layer significantly improved in diabetic retina. (**F**) Complement C3 (*red*) and C5b-9 (*red*) were mainly distributed within the deposits (*dotted line* area) in the diabetic retina, but not in controls. *Scale bar:* 50 μm.

(Fig. 5A, arrows). They were pink doom-shaped and laminal sub-RPE deposits with varied sizes (Figs. 5B–5D, dotted line). Above the druseniond lesions, the counterpart RPE cells were hyperpigmented and hypertropy, indicating the possibly concomitant damage to the RPE cells. Moreover, ApoE, alpha-crystallin B chain (CRYAB), C3 and C5b-9, the critical components found in human drusen, were detected in diabetic monkeys and controls by immunofluorescence (Figs. 5E and 5F). While the RPE65+ RPE cells in controls were continuous and regular, the RPE cells in diabetic monkeys exhibited discrete and dotted shape. Remarkably, extensive C5b-9 and C3 were found within the deposits in diabetic retina but not in controls (Fig. 5F). It is worth noting that, CRYAB was specifically detected in the RPE cells overlying the deposits, indicating that the RPE cells were under oxidative stress (Fig. 5E). ApoE, enriched in RPE cells and a common component of deposits, accumulated in the diabetic RPE cells whereas not located within the deposits (Fig. 5E). Furthermore, the expression level of main complement components like C3 and C4 in plasma was detected. The plasma level of C3 and C4 was increased significantly in diabetic monkeys with drusen compared with nondiabetic controls ($P = 0.028$ and $P = 0.029$, respectively) (Fig. 6). In addition, the lipid profile including LDL, triglyceride, and total cholesterol were found to be slightly increased but with no statistically significant difference in the Drusen-positive subgroup of diabetic monkeys in comparison to Drusen-negative ones (Supplementary Fig. S2). The blood glucose and HbA1c had no statistically significant differences between these subgroups

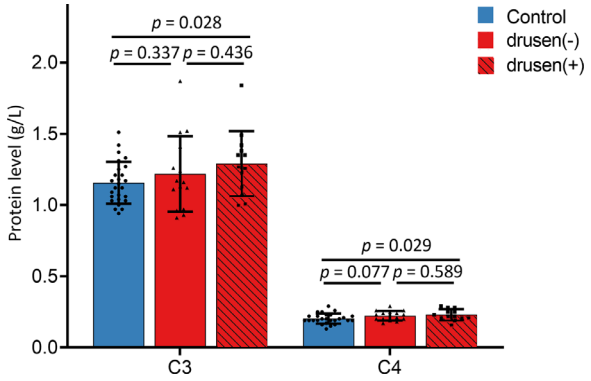

Figure 6. Systemic complement level was particularly increased in diabetic monkey with drusen lesions. Although the plasma level of C3 was not increased in diabetic monkeys without drusen compared with nondiabetic controls ($P = 0.337$), C3 expression has a significant elevation in diabetic monkeys with drusen lesions ($P = 0.028$). Similarly, plasma C4 expression was increased in diabetic monkeys, particularly in those with drusen lesions ($P = 0.029$). n = 26 controls, n=15 diabetic monkeys without drusen, n = 13 diabetic monkeys with drusen.

in the diabetic monkeys, indicating that the glycemic control was less likely to be involved in drusen development. These results suggested that local and systemic complement activation might be involved in diabetic drusenoid lesion formation.

Discussion

In this study, we conducted a research in a large group of 54 cynomolgus monkeys after screening more than 800 monkeys and described a distinctive landscape of early diabetic retinopathy in NHP models. We found the typical neural injury and histopathological change of retinal vasculature in these NHP diabetic models. Particularly, a featured druseniod sign was also recognized, establishing a distinctive pathological spectrum of early-stage DR in NHP models. These sub-RPE drusen-like lesions were identified as complement deposition, which possibly derived from diabetic RPE cells and circulation. Our results broaden the phenotype understanding of early-stage DR in NHP models and provided evidence that RPE may contribute to the pathological change of DR.

To the best of our knowledge, this is the first report of early-stage retinopathy spectrum in spontaneous diabetes NHP model with a large sample size (28 DM and 26 controls). Buchi et al. observed vascular leakage, intraretinal exudates and hemorrhage, and cystoid degeneration in six diabetic monkeys (two spontaneous and four induced by streptozocin).[9] Kim et al. reported signs of DR such as capillary dropout, large-vessel pruning, cotton-wool spots, and microaneurysms in 16 spontaneous diabetic monkeys, in spite of no CFP, FFA, or OCT images from this publication.[10] Here we applied multimodal imaging to examine the retinopathy of 28 diabetic monkeys. Although our DR NHP models did not present any of the above-described signs maybe due to shorter diabetes duration (medical record of 3-5 years), we provided a limited early-stage DR model with neural and vascular damage. As far as we known, except from genetically modified rodents, only NHP could develop spontaneous type 2 diabetes, associated with age and body weight increase.[2–4] Compared with diet-induced diabetic NHP models, which were reported to exhibit pericyte loss and abnormal retinal vascular permeability within two years,[19] this spontaneous NHP usually developed retinopathy after a longer follow-up. Further investigation with longer follow-up is extremely important. Since retinal angiogenesis, the hallmark of proliferative DR in humans, has never been reported in diabetic NHP models,[9–11,19] the discrepancy of NHP and humans still need to be concerned when using NHP models. In addition, since only three monkeys per group were used for histological and molecular analysis, more samples are needed for further investigation.

Normal aged monkeys may develop drusenoid deposits sporadically.[20–22] In humans, drusen progressively appears as aging and associates with AMD. It is reported that the development of drusen increases a person's risk for development of AMD, although it not be the cause of AMD.[23,24] Considering the association between diabetes with AMD, some studies have suggested an increased risk for advanced AMD in diabetes patients.[25–28] Consistently in this study, diabetic NHP presented a higher incidence of drusenoid deposition compared to age-matched ones. Here we found the diabetic RPE cells highly expressed genes of complement activation, inflammatory signaling and cytokines, which inclined to influence the adjacent Bruch's membrane and chroidal circulation, may predispose to the development of AMD. The increased blood glucose levels, impaired glucose tolerance, and more advanced glycation end products facilitated the emergence of macular RPE abnormalities. So the changes in the structure and function of RPE cells are probably the early features of both DR and AMD.

DR is generally considered to mainly involve the inner retina, where the inner blood-retinal barrier is located.[29] Consistent with previous study, our data showed that both Müller cells and microglia were activated in response to diabetes insult with strong staining of GFAP and Iba1 in the diabetic retinae, indicating glia activation in the inner retina involved in the DR and featured DR as neurodegenerative process. Here, the RPE cell, the critical component of outer blood-retinal barrier, was also found to be injured during DR development.[30–33] The RPE cell is one of the major sources of local complement in the retina.[34] We found sub-RPE drusenoid lesion in the diabetic NHP required complement activation, which may establish a chronic inflammatory circumstance. In this study, we also found that some chemokines, including Ccl26, ccl13, ccl18, and ccl17, were enriched and ranked as top 50 upregulated genes in diabetic RPE cells, indicating that inflammation was involved and recruitment of the immune cells might play an important role. Other upregulated genes included those involved in cell death, such as ripk3, Gsdma, Birc7, suggesting the important links of cell death. In addition, the breaking down of the blood retinal barrier in DR has been reported to facilitate the leakage of circulating complement proteins into retina, inducing a cascade response of complement activation. Consistently, the elevation of systemic C3 and C4 was observed in diabetic monkeys with drusenoid lesions but not in the diabetic ones without drusenoid lesions. Nevertheless, no statistical significance was observed between diabetic animals with and without drusenoid lesions, which might be due to the limited animal numbers. Furthermore, the pathogenesis of diabetes has been known to be extremely complicated. More pathological factors should be investigated to strengthen the hypothesis and uncover potential mechanism beyond complement system in future study.

Investigative Ophthalmology & Visual Science

Previous studies showed the deposition of C5b-9 in the wall of retinal vessels of human eye donors with type 2 diabetes,[35] and the complement factors C3, C4b, C9 and factor B were found to be highly produced in the vitreous humor of DR patients.[36] So it is speculated that the complement abnormality and RPE damage comprise a vicious circle during the pathological process of DR.

In conclusion, this study provided a panorama of early-stage DR in NHP models and featured it with characterized vascular and neural damage and a distinctive drusenoid lesion. Although it could not mimic the entire DR process, this diabetic NHP model exhibited special early-stage histopathological abnormality of DR, indicating it as an available and appropriate model for limited early-stage DR. We also demonstrated complement abnormality in RPE cells and in systems contributed to the development of early-stage DR, providing evidence of an unrecognized role of RPE cells, which might be helpful to better understand the molecular basis of early-stage DR.

Acknowledgments

Supported by National Key R&D Program of China (No. 2018YFA0108300), National Natural Science Foundation of China (No. 81630022, 81700825), Natural Science Foundation of Guangdong Province, China (No. 2019B151502006), and Science and Technology Program of Guangzhou, China (No. 201906010076, 201707020006).

Disclosure: **S. Fan,** None; **Z. Yang,** None; **Y. Liu,** None; **J. Zhong,** None; **S. Zhang,** None; **Y. Xiao,** None; **X. Liu,** None; **W. Yi,** None; **C. He,** None; **Y. Hu,** None; **X. Liu,** None

References

1. Solomon SD, Chew E, Duh EJ, et al. Diabetic retinopathy: a position statement by the American Diabetes Association. *Diabetes Care*. 2017;40:412–418.
2. Robinson R, Barathi VA, Chaurasia SS, Wong TY, Kern TS. Update on animal models of diabetic retinopathy: from molecular approaches to mice and higher mammals. *Dis Model Mech*. 2012;5:444–456.
3. Cefalu WT. Animal models of type 2 diabetes: clinical presentation and pathophysiological relevance to the human condition. *ILAR J*. 2006;47:186–198.
4. Howard CF. Diabetes in macaca nigra: metabolic and histologic changes. *Diabetologia*. 1974;10(Suppl 1):671–677.
5. Thomson SE, McLennan SV, Kirwan PD, et al. Renal connective tissue growth factor correlates with glomerular basement membrane thickness and prospective albuminuria in a non-human primate model of diabetes: possible predictive marker for incipient diabetic nephropathy. *J Diabetes Complications*. 2008;22:284–294.
6. Thomson SE, McLennan SV, Hennessy A, et al. A novel primate model of delayed wound healing in diabetes: dysregulation of connective tissue growth factor. *Diabetologia*. 2010;53:572–583.
7. Fan S, Ding X, Rao P, et al. Multimodal imaging of the retina and choroid in healthy macaca fascicularis at different ages. *Graefes Arch Clin Exp Ophthalmol*. 2019;257:455–463.
8. Peng Y, Shekhar K, Yan W, et al. Molecular classification and comparative taxonomics of foveal and peripheral cells in primate retina. *Cell*. 2019;176:1222–1237.
9. Büchi ER, Kurosawa A, Tso MO. Retinopathy in diabetic hypertensive monkeys: a pathologic study. *Graefes Arch Clin Exp Ophthalmol*. 1996;234:388–398.
10. Kim SY, Johnson MA, McLeod DS, et al. Retinopathy in monkeys with spontaneous type 2 diabetes. *Invest Ophthalmol Vis Sci*. 2004;45:4543–4553.
11. Johnson MA, Lutty GA, McLeod DS, et al. Ocular structure and function in an aged monkey with spontaneous diabetes mellitus. *Exp Eye Res*. 2005;80:37–42.
12. Wilkinson CP, Ferris FL, Klein RE, et al. Proposed international clinical diabetic retinopathy and diabetic macular edema disease severity scales. *Ophthalmology*. 2003;110:1677–1682.
13. Chew Y. E. Association of elevated serum lipid levels with retinal hard exudate in diabetic retinopathy. *Arch Ophthalmol*. 1996;114:1079–1084.
14. Kim SY, Johnson MA, McLeod DS, et al. Neutrophils are associated with capillary closure in spontaneously diabetic monkey retinas. *Diabetes*. 2005;54:1534–1542.
15. Spraul CW. Characteristics of drusen and bruch's membrane in postmortem eyes with age-related macular degeneration. *Arch Ophthalmol*. 1997;115:267–273.
16. Nozaki M, Raisler BJ, Sakurai E, et al. Drusen complement components c3a and c5a promote choroidal neovascularization. *Proc Natl Acad Sci U S A*. 2006;103:2328–2333.
17. Anderson DH, Mullins RF, Hageman GS, Johnson LV. A role for local inflammation in the formation of drusen in the aging eye. *Am J Ophthalmol*. 2002;134:411–431.
18. Chou JC, Rollins SD, Fawzi AA. Trypsin digest protocol to analyze the retinal vasculature of a mouse model. *J Vis Exp*. 2013;(76):e50489.
19. Chronopoulos A, Roy S, Beglova E, et al. Hyperhexosemia-induced retinal vascular pathology in a novel primate model of diabetic retinopathy. *Diabetes*. 2015;64:2603–2608.
20. Umeda S, Suzuki MT, Okamoto H, et al. Molecular composition of drusen and possible involvement of anti-retinal autoimmunity in two different forms of macular degeneration in cynomolgus monkey (macaca fascicularis). *FASEB J*. 2005;19:1683–1685.
21. Mullins RF, Hageman GS. Histochemical comparison of ocular "drusen" in monkey and human. In: *Degenerative retinal diseases*. Boston: Springer; 1997: 1–10.
22. Stafford TJ, Anness SH, Fine BS. Spontaneous degenerative maculopathy in the monkey. *Ophthalmology*. 1984;91(5):513–521.
23. Wang JJ, Foran S, Smith W, Mitchell P. Risk of age-related macular degeneration in eyes with macular drusen or hyperpigmentation: the blue mountains eye study cohort. *Arch Ophthalmol*. 2003;121:658–663.
24. Klein R, Klein BE, Tomany SC, Meuer SM, Huang GH. Ten-year incidence and progression of age-related maculopathy: the beaver dam eye study. *Ophthalmology*. 2002;109:1767–1779.
25. He M, Chang F, Lin H, et al. The association between diabetes and age-related macular degeneration among the elderly in Taiwan. *Diabetes Care*. 2018;41:2202–2211.
26. Choi JK, Lym YL, Moon JW, Shin HJ, Cho B. Diabetes mellitus and early age-related macular degeneration. *Arch Ophthalmol*. 2011;129:196–199.
27. Hahn P, Acquah K, Cousins SW, Lee PP, Sloan FA. Ten-year incidence of age-related macular degeneration according to diabetic retinopathy classification among medicare beneficiaries. *Retina (Philadelphia, Pa.)*. 2013;33:911–919.
28. Topouzis F, Anastasopoulos E, Augood C, et al. Association of diabetes with age-related macular degeneration in the EUREYE study. *Br J Ophthalmol*. 2009;93:1037–1041.
29. Klaassen I, Van Noorden CJ, Schlingemann RO. Molecular basis of the inner blood-retinal barrier and its breakdown in diabetic macular edema and other pathological conditions. *Prog Retin Eye Res*. 2013;34:19–48.

30. Decanini A, Karunadharma PR, Nordgaard CL, et al. Human retinal pigment epithelium proteome changes in early diabetes. *Diabetologia*. 2008;51:1051–1061.
31. Weinberger D, Fink-Cohen S, Gaton DD, Priel E, Yassur Y. Non-retinovascular leakage in diabetic maculopathy. *Br J Ophthalmol*. 1995;79:728–731.
32. Soliman W, Sander B, Jørgensen TM. Enhanced optical coherence patterns of diabetic macular oedema and their correlation with the pathophysiology. *Acta Ophthalmol Scand*. 2007;85:613–617.
33. Vinores SA, Gadegbeku C, Campochiaro PA, Green WR. Immunohistochemical localization of blood-retinal barrier breakdown in human diabetics. *Am J Pathol*. 1989;134:231–235.
34. Pauly D, Agarwal D, Dana N, et al. Cell-type-specific complement expression in the healthy and diseased retina. *Cell Reports*. 2019;29:2835–2848.
35. Zhang J, Gerhardinger C, Lorenzi M. Early complement activation and decreased levels of glycosylphosphatidylinositol-anchored complement inhibitors in human and experimental diabetic retinopathy. *Diabetes*. 2002;51:3499–3504.
36. García-Ramírez M, Canals F, Hernández C, et al. Proteomic analysis of human vitreous fluid by fluorescence-based difference gel electrophoresis (DIGE): a new strategy for identifying potential candidates in the pathogenesis of proliferative diabetic retinopathy. *Diabetologia*. 2007;50:1294–1303.

Investigative Ophthalmology & Visual Science